Terahertz generation from ZnTe optically pumped above and below the bandgap

Dongwei Zhai, Emilie Hérault, Frédéric Garet, Jean-Louis Coutaz

Research Article | Vol. 29, No. 11 / 24 May 2021 / Optics Express 17491
Optics EXPRESS

Terahertz generation from ZnTe optically pumped above and below the bandgap

DONGWEI ZHAI,* EMILIE HÉRAULT, FRÉDÉRIC GARET, AND JEAN-LOUIS COUTAZ

IMEP-LAHC, UMR CNRS 5130, University Savoie Mont Blanc, 73 376 Le Bourget du Lac Cedex, France
**dongwei.zhai@univ-smb.fr*

Abstract: We report on the generation of THz waves through optical rectification in ZnTe of femtosecond laser pulses whose photon energy is tuned from below to above the ZnTe bandgap energy. The THz signal exhibits a pronounced peak at the bandgap energy, at THz frequencies for which losses in ZnTe remain small. This peak is likely due to the resonance of the ZnTe nonlinear susceptibility in the vicinity of the bandgap.

1. Introduction

Optical rectification (OR) of femtosecond laser pulses in electrooptic crystals is an elegant way to produce broadband and powerful terahertz (THz) pulses [1–2]. The OR optical-THz conversion efficiency is governed [3] by the crystal nonlinearity, its losses at both optical and THz frequencies, and the possibility of achieving phase-matching. When using common Ti:Sapphire mode-locked lasers emitting at 0.8-µm wavelength, ZnTe is an excellent material [4–5], because phase-matching is almost realized, losses are rather weak, and the birefringence issue is ignored, even if its nonlinear coefficients are quite small as compared to the ones of other employed crystals ($LiNbO_3$, $LiTaO_3$...) [6]. Making larger the nonlinear coefficients is possible by tuning the laser pump wavelength closer to the bandgap [7–8]. However, optical losses increase as well, leading to a decrease of the THz generated signal. When the pumping photon energy is larger than the bandgap (2.3 eV), excitation of free carriers in the conduction band of ZnTe occurs. Under normal incidence, these free carriers do not contribute to the THz generation, and thus the observed THz signal is still emitted by bound electrons. In this paper, we report on THz emission from a ZnTe crystal excited by optical pulses delivered by an optical parametric amplifier, whose wavelength is tuned from 800 nm down to 476 nm, corresponding to a photon energy varying from 1.55 eV to 2.60 eV, that is below and above the ZnTe bandgap.

2. Experimental methods

The ZnTe wafer is 1.52-mm thick and [111] oriented. It serves as an emitting THz antenna in a common THz time-domain setup. The THz signal is collected by two parabolic mirrors and directed towards an electrooptic detection system, which includes a 0.5-mm [110] ZnTe crystal, a Wollaston prism and a balanced photodiodes detector. An amplified Ti:Sapphire mode-locked laser (Coherent Libra 7) supplies 45-fs pulses of 0.8-µm wavelength at a 1-kHz repetition rate. A part of the beam feeds an OPA (Topas from Light Conversion) that delivers 50-fs pulses whose wavelength is presently tuned from 476 to 800 nm (i.e. from 2.60 to 1.55 eV). The OPA output beam is mechanically chopped and excites the ZnTe emitter under normal incidence. The detector is synchronously triggered by pulses from the mode-locked laser and the THz waveform is read with a lock-in amplifier. The experiment is performed in dehydrated air (8% humidity) and at room temperature.

At the crystal, the focused spot diameter is 2 mm. Due to the limitation of nonlinear efficiency in OPA, its average power is 10 mW in the range 1.55-2.60 eV (peak power density 6.37 GW/cm^2).

#421282 https://doi.org/10.1364/OE.421282
Journal © 2021 Received 1 Feb 2021; revised 11 Apr 2021; accepted 12 Apr 2021; published 21 May 2021

Optics EXPRESS

After the ZnTe emitter, a Teflon plate blocks the remaining OPA light. The exciting laser beam is linearly polarized along the [$\bar{1}$10] axis of the crystal and thus the generated THz beam is also linearly polarized along the same direction [9].

3. Results and discussion

Figure 1 shows the THz waveforms recorded for different pumping photon energies. For the sake of visibility, each waveform is vertically shifted by 1 as compared to the neighbor curve below. The respective pumping photon energy is given on the right side. For energies below the bandgap, the waveform curves exhibit the typical THz dipolar pulse due to the mismatch between the THz and optical velocities, followed by damped oscillations originating in dispersion at THz frequencies [10]. The penetration depth is greater than the crystal length (3.2 mm at 1.55 eV or 1.6 mm at 1.84 eV for example). Near the bandgap, the penetration depth shortens to few hundreds of micrometers (330 μm at 2.30 eV, 160 μm at 2.33 eV for example), and over the bandgap, its value is down to a few hundred of nanometers. The oscillations are erased as the optical pulse no more propagates in the crystal.

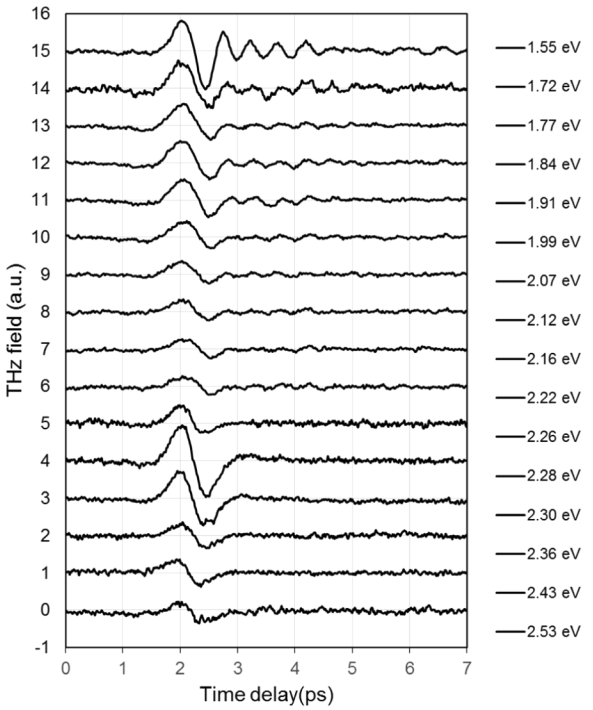

Fig. 1. THz waveforms recorded for different pumping photon energies (values given on the right side). For the sake of legibility, each plot is vertically shifted by 1 as compared to the neighbor one below.

The corresponding spectra are depicted in Fig. 2. For the sake of legibility, only the spectra obtained for pumping energies of 1.55, 1.91, 2.26 and 2.30 eV are plotted. In the transparency range of ZnTe, the spectra are limited to 1~3 THz because of the rather large thickness of the ZnTe sample that serves as THz emitter. Typically, this bandwidth slightly decreases when the pump photon energy gets closer to the bandgap energy. Above the bandgap energy, the spectra shape changes. At these energies, the penetration depth is short. The THz signal is generated only at the input surface of the crystal, since the pump beam is strongly absorbed. The THz wave, as it propagates, is then absorbed all along the crystal. The absorption is quite small for the

Optics EXPRESS

lowest energies. However, as the absorption increases with the frequency, the highest frequencies vanish from the emitted spectrum.

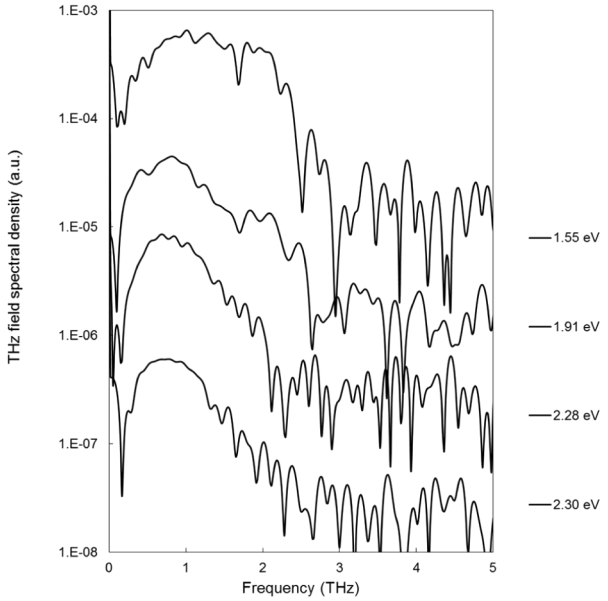

Fig. 2. Spectra of the THz waveforms plotted in Fig. 1, recorded for different pumping photon energies (values given on the right side). For the sake of legibility, each plot is vertically shifted by 1 decade as compared to the neighbor one below.

Plotting (Fig. 3) the experimental data for a given THz frequency versus the pumping photon energy reveals some amazing results. When the photon energy increases from 1.5 eV up to 2.2 eV (range of transparency of ZnTe), the THz signal decreases whatever is the THz frequency (except the 1.55-eV value at 0.36 THz. Let us notice that the experimental uncertainty is quite large at 0.36 THz and smaller frequencies, because of the weak generated signal – see Fig. 2). A strong peak is observed at 2.3 eV for THz frequencies up 1.5 THz, over which this peak disappears. Its spectral width is about 0.15 eV. At larger photon energies, the THz signal strongly declines. This is clearly seen for the 0.8-THz case, for which the peak is well contrasted as compared to the baseline. At higher THz frequencies, the peak can no longer be distinguished. This can be explained by the fact that absorption is stronger for high terahertz frequencies. The possible enhancement is then canceled by this absorption. Figure 4 allows the comparison between the enhancement peak and the crystal absorption between 2 eV and 2.4 eV. Absorption was extracted from spectroscopic measurements with a Shimadzu UV-2600 spectrometer in transmission and reflection thanks to the formula [11]:

$$\alpha(\lambda) = -\frac{1}{d}\ln\left(\frac{-(1-R(\lambda))^2 + \sqrt{(1-R(\lambda))^4 + 4\,T(\lambda)^2\,R(\lambda)^2}}{2\,T(\lambda)R(\lambda)^2}\right) \tag{1}$$

where λ is the wavelength, d is the crystal thickness, $R(\lambda)$ and $T(\lambda)$ are respectively the measured reflectance and transmittance. The absorption edge of ZnTe is clearly seen on the absorption spectrum. Over 2.3 eV, the absorption plateau at about 65 cm^{-1} is an artefact due to the lack of transmitted signal, which makes $T(\lambda)$ substituted by noise in (1).

We can see on Fig. 4 that the peak position corresponds to the beginning of the absorption edge. For higher photon energies, the THz signal decreases rapidly. This could be due to THz

Optics EXPRESS

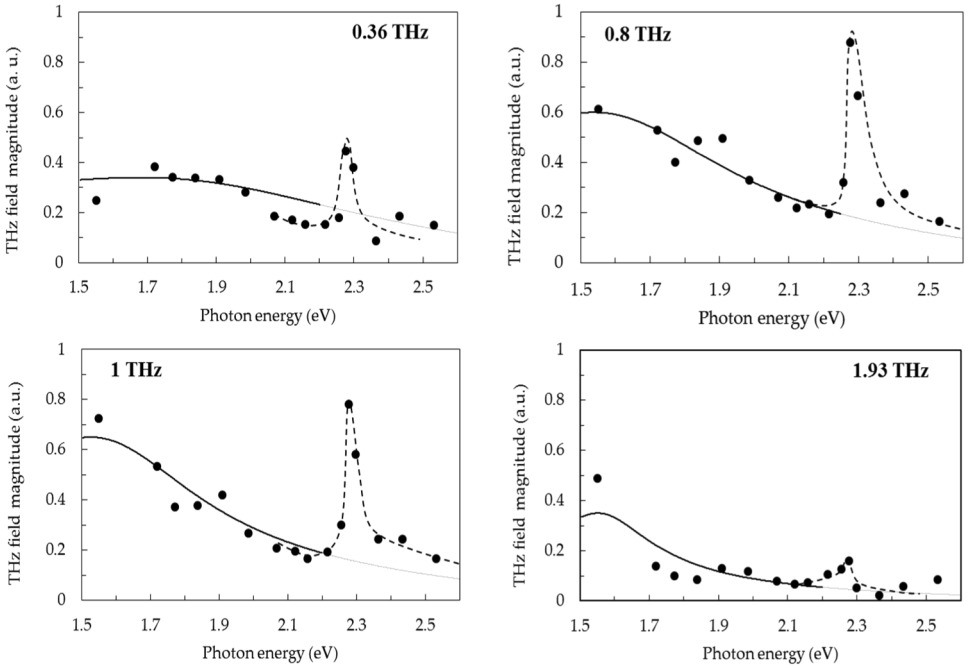

Fig. 3. THz field magnitude at 0.36, 0.8, 1 and 1.93 THz versus the pumping photon energy. Full circles are experimental data. The lines are calculated with expression (1), and are continuous in the range of validity (1.5-2.2 eV). For information, they are plotted as dashed lines over 2.2 eV, even if the calculation is no more valid. The dotted line is a guide to the eyes that emphasizes the 2.3-eV peak.

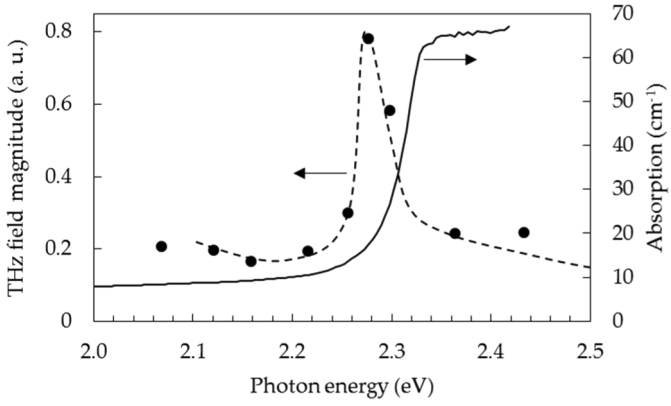

Fig. 4. THz field magnitude at 1 THz and crystal absorption versus the pumping photon energy. Full circles are experimental data. The dotted line is a lead to the eye.

Optics EXPRESS

absorption by the photo-generated free carriers. Indeed, the pump fluence here is 0.3 mJ/cm^2, well below the saturation threshold of free carriers in ZnTe measured by Ku *et al*. [12]. Also, the penetration depth decreasing rapidly at high photon energies, only a small part of the crystal length is used for the THz generation. Finally, the optical photons used to generate free carriers do not contribute to the nonlinear optical process of THz conversion, limiting the efficiency.

Figure 5 presents the THz field magnitude versus the THz frequency for different photon energies below the bandgap (1.95 and 2.15 eV), at the bandgap (2.28 eV) and above the bandgap (2.5 eV). These values are normalized to the one at 1.55 eV, in order to get rid of the spectral shape of the THz signal due to both the laser pulse duration and the detection bandwidth. Below the bandgap (1.95 and 2.15 eV), the normalized signal slightly decreases with the THz frequency. Above 1.5~1.7 THz, it becomes noisy due to the weakness of the recorded signals. At the bandgap, the result is very different as compared to below the bandgap: a peak clearly appears around 0.55 THz. At higher frequencies, the signal gently decreases. At 2.53 eV, another behavior is observed: the signal increases gradually and monotonously with the frequency, without any peak. In the transparency range of ZnTe, i.e. below the bandgap, THz generation originates in OR. The expression of the amplitude of the THz field radiated outside the crystal of thickness x is given by [3,13]:

$$\vec{E}_\Omega(x) = \frac{\Omega^2}{c^2} \times \frac{2(n_\Omega + j\kappa_\Omega)}{n_\Omega + 1 + j\kappa_\Omega} \times \frac{4}{(1+n_\omega)^2 + {\kappa_\omega}^2} \times \frac{\left(\overleftrightarrow{\chi}^{(2)} : \vec{E}_{\omega+\Omega} \cdot \vec{E}^*_\omega\right)}{\frac{\Omega}{c}(n_\Omega + n_{G,\omega}) + j\left(\frac{\alpha_\Omega}{2} + \alpha_\omega\right)} L_{gen}, \tag{2}$$

with:

$$L_{gen} = \frac{e^{j\frac{\Omega}{c}n_\Omega x} e^{-\frac{\alpha_\Omega}{2}x} - e^{j\frac{\Omega}{c}n_{G,\omega}x} e^{-\alpha_\omega x}}{\frac{\Omega}{c}(n_\Omega - n_{G,\omega}) + j\left(\frac{\alpha_\Omega}{2} - \alpha_\omega\right)}. \tag{3}$$

Expression (2) is valid for plane waves and within the hypothesis of neglecting rebounds of both THz and optical beams inside the crystal. Ω and ω are respectively the THz and optical angular frequencies, α_Ω and α_ω are the coefficients of absorption, κ_Ω and κ_ω the coefficients of extinction, n_Ω and n_ω are the refractive indices. $n_{G,\omega}$ is the group index at optical frequency. $\overleftrightarrow{\chi}^{(2)}$ is the nonlinear tensor of the crystal corresponding to the photon interaction $(\omega + \Omega) - \omega \rightarrow \Omega$ (in zinc-blende crystals like ZnTe, only the $\chi^{(2)}_{14} = \chi^{(2)}_{25} = \chi^{(2)}_{36}$ elements of the tensor are not null), and $\vec{E}_\omega$ is the field of the pumping laser beam outside the crystal. The term L_{gen} has the dimension of a length and its modulus $|L_{gen}|$, called "the effective generation length" [14,3], renders for the propagation effects, especially the phase-matching process. The spectral features of the THz field amplitude are also strongly governed by the ones of the nonlinear tensor. In view of determining the spectral dependence of the nonlinear tensor, we use the classical anharmonic oscillator model [15,3] that leads to:

$$\chi^{(2)} \propto \chi^{(1)}(\Omega)|\chi^{(1)}(\omega)|^2 \tag{4}$$

In this expression, we write only the order of magnitude $\chi^{(i)}$ (i=1,2) of the tensor $\overleftrightarrow{\chi}^{(i)}$. $\chi^{(1)}$ denotes the linear tensor that is linked to the complex refractive index by $(n + j\kappa)^2 = 1 + \chi^{(1)}$.

We compute the THz field strength outside the crystal using expressions (2), (3) and (4). The requested refractive indices and absorption coefficients of ZnTe are taken from Marple [16] (n_ω), Horikoshi *et al.* [17] (α_ω), and Gallot *et al.* [18] (n_Ω and α_Ω). No adjustable parameter is used in the calculation, except the optical absorption α_ω that strongly depends on the ZnTe growth process [17] and is known to change from a sample to another one. However, its value remains almost constant [17] from 1.5 up to 2.2~2.3 eV whatever is the sample. Thus, we state it, in the calculation, as a constant independent of the optical frequency and we only adjust its value to get the best fits. The results of the calculation are plotted as continuous lines in Fig. 3. The fits of the

Optics EXPRESS

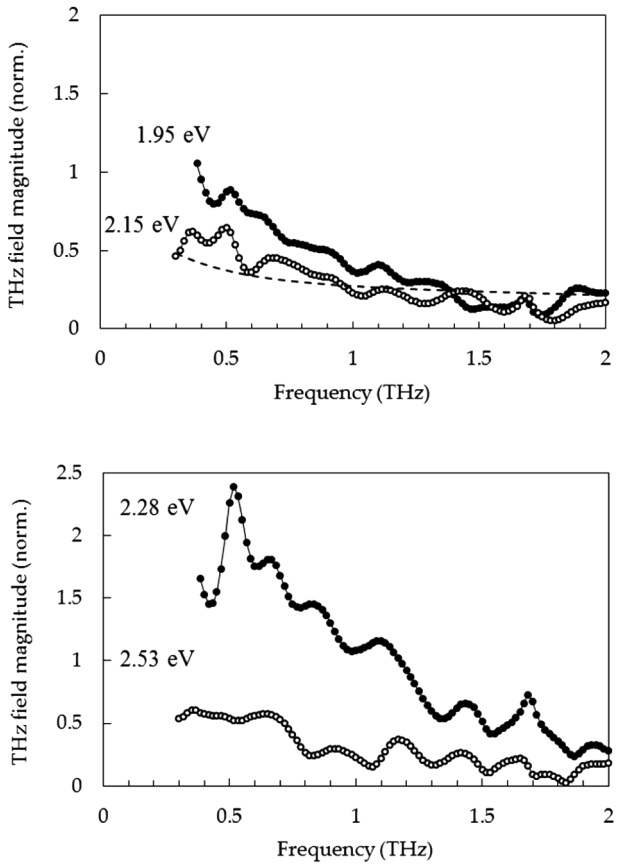

Fig. 5. THz field magnitude normalized to the 1.84-eV value versus THz frequency, for photon energies below the bandgap (1.95 and 2.15 eV), at the bandgap (2.28 eV), and above the bandgap (2.53 eV). The dashed line is a fit of 2.15-eV data using expressions (1), (2) and (3).

experimental data, whatever is the THz frequency, are quite good up to ~2.2 eV. For information, we plot the curves as dotted lines above 2.2 eV, i.e. in the absorption range of ZnTe, where the calculation is no more valid. We also plot the calculated curve for the 2.15-eV case with exactly the same parameters as for the fits of Fig. 3. Here again, the model matches with a rather good accuracy the measured data.

The best fits for all the plots are obtained for α_ω = 60 cm^{-1}, which is about 6 times larger than reported by Horikoshi *et al.* [17]. This discrepancy may be explained by a two-photon absorption effect, because, as stated above, the peak power density of the pumping laser beam is quite high (6.37 GW/cm^2). According to Schall and Uhd-Jepsen [19], the TPA coefficient of ZnTe is $\beta \approx 5.5$ cm/GW when the crystal is pumped at 800 nm at a temperature of 10 K. This leads to a TPA-induced absorption equal to 35-40 cm^{-1}, which added to the measured intrinsic absorption of about 5-10 cm^{-1} in the range 0.5~2 eV, gives a total absorption of 40-50 cm^{-1}. This is of the order of magnitude of the 60 cm^{-1} value deduced from the fits of Fig. 3. The higher experimental value is certainly due to the fact that we perform the experiment at room temperature, at which β is larger than at cryogenic temperatures [20].

The model reveals that the decline of the THz signal from 1.5 eV up to 2.2 eV is due to a diminution of L_{gen} as its denominator increases because of a larger optical dispersion closer to

Optics EXPRESS

the bandgap. This calculation, performed again without any adjustable variable, allows us to fit rather well the experimental THz spectra for photon energy below the bandgap (see Fig. 5).

To our knowledge, $\overleftrightarrow{\chi}^{(2)}((\omega+\Omega)-\omega\rightarrow\Omega)$ has never been theoretically addressed in semiconductors near or above the bandgap energy, but the dispersion of the second harmonic generation (SHG) tensor $\overleftrightarrow{\chi}^{(2)}(\omega+\omega\rightarrow 2\omega)$ was subject to intense researches [21,22,23,7]. Second-order perturbation calculation describes fairly well the experimental SHG records for zinc-blende semiconductors [24], even if the experimental data are scarce [25]. Moreover, when inter-band transition between the highest levels of the valence band and the lowest levels of the conduction band is the major photo-excitation process, the SHG tensor can be approximated as a combination of the linear susceptibilities at ω and 2ω [26]. Thus, the measured dispersion of $\chi_{14}^{(2)}(\omega+\omega\rightarrow 2\omega)$ in InAs and InSb (see Fig. 1 in Ref. [27]) exhibits a shape very similar to the one of the THz signal presented here (for example Fig. 3 at 0.8 THz), with a decrease with photon energy in the range below the bandgap, and a pronounced peak at the bandgap. Therefore, because of the similar physical origin of SHG and OR phenomena, it is likely that the THz peak at 2.3 eV originates in the resonant nonlinearity. The lessening of the peak at higher THz frequencies may be explained by the larger losses at these frequencies, which dump the resonance effect. As compared to SHG, excitation of ZnTe above the bandgap creates free carriers that interact strongly with the generated THz beam. Especially, carriers generated by the first coming part of the laser pulse absorb the THz radiation. All these hypotheses must be confirmed by a theoretical study.

Another explanation for the peak observed at 2.3 eV could be phase-matching. Phase-matching occurs in lossy materials when both equalities $n_\Omega = n_{G,\omega}$ and $\alpha_\Omega = 2\alpha_\omega$ are fulfilled. Let us notice that phase-matching cannot be realized when the optical beam is strongly absorbed, because of inter-band transitions, since the optical decay length becomes shorter than the THz wavelength. Therefore phase-matching effect is expected to be observed in the transparency range of ZnTe, or in the very proximate vicinity of the bandgap energy. To check this hypothesis, we use, in the transparency range, ZnTe parameters from Marple [16] and Horikoshi *et al.* [17] as explained above. In the absorption range, i.e. above the bandgap, data from Sato *et al.* [28] are very reliable. Again, we employ THz data from Gallot *et al.* [18]. Phase-matching with a 2.3-eV photon energy is calculated to be achieved around 5 THz. For all the photon energies addressed during the current measurement (from 1.55 eV to 2.56 eV), phase-matching is calculated to appear outside the ~3-THz bandwidth allowed by the 1.52-mm thickness of the sample, and thus its effect cannot be observed.

4. Conclusion

In conclusion, THz emission through optical rectification in ZnTe exhibits a contrasted peak when the pumping photon energy is of the order the ZnTe bandgap energy, and for THz frequencies within the range of weak absorption of the crystal. It is probable that this peak results from the bandgap resonance of the ZnTe nonlinear susceptibility. This hypothesis must be confirmed by theoretical works.

Funding. Ministry of Science and Technology, Taiwan; Agence Nationale de la Recherche (ANR-17-CE24-0031-01).

Disclosures. The authors declare no conflicts of interest.

References

1. B. B. Hu, X.-C. Zhang, and D. H. Auston, "Free-space radiation from electro-optic crystals," Appl. Phys. Lett. **56**(6), 506–508 (1990).
2. Q. Tian, H. Xu, Y. Wang, Y. Liang, Y. Tan, X. Ning, L. Yan, Y. Du, R. Li, J. Hua, W. Huang, and C. Tang, "Efficient generation of a high-field terahertz pulse train in bulk lithium niobate crystals by optical rectification," Opt. Express **29**(6), 9624–9634 (2021).
3. A. Schneider, M. Neis, M. Stillhart, B. Ruiz, R. U. A. Khan, and P. Günter, "Generation of terahertz pulses through optical rectification in organic DAST crystals: theory and experiment," J. Opt. Soc. Am. B **23**(9), 1822–1835 (2006).

Optics EXPRESS

4. Q. Wu and X.-C. Zhang, "Design and characterization of traveling-wave electrooptic terahertz sensors," IEEE J. Sel. Top. Quantum Electron. **2**(3), 693–700 (1996).
5. M. Cornet, J. Degert, E. Abraham, and E. Freysz, "Terahertz-field-induced second harmonic generation through Pockels effect in zinc telluride crystal," Opt. Lett. **39**(20), 5921–5924 (2014).
6. R. W. Boyd, "Nonlinear Optics," 3rd edition, Associated Press, p. 517, 2008.
7. C. Y. Fong and Y. R. Shen, "Theoretical studies on the dispersion of the nonlinear optical susceptibilities in GaAs, InAs, and InSb," Phys. Rev. B **12**(6), 2325–2335 (1975).
8. X. C. Zhang, Y. Jin, K. Yang, and L. J. Schowalter, "Resonant nonlinear susceptibility near the GaAs band gap," Phys. Rev. Lett. **69**(15), 2303–2306 (1992).
9. F. Sanjuan, G. Gaborit, and J.-L. Coutaz, "Full electro-optic terahertz time-domain spectrometer for polarimetric studies," Appl. Opt. **57**(21), 6055–6060 (2018).
10. A. Schneider, "Theory of terahertz pulse generation through optical rectication in a nonlinear optical material with a finite size," Phys. Rev. A **82**(3), 033825 (2010).
11. J. Gervais, "Mesure du coefficient d'absorption optique dans le silicium multicristallin de type P pour photopiles solaires," J. Phys. III **3**(7), 1489–1495 (1993).
12. S. A. Ku, C. M. Tu, W.-C. Chu, C. W. Luo, K. H. Wu, A. Yabushita, C. C. Chi, and T. Kobayashi, "Saturation of the free carrier absorption in ZnTe crystals," Opt. Express **21**(12), 13930–13937 (2013).
13. J.-L. Coutaz, F. Garet, and V. P. Wallace, "Principles of Terahertz time-domain spectroscopy," Chapter 7, Pan Stanford Publishing, 2018.
14. N. C. J. van der Valk, P. C. M. Planken, A. N. Buijserd, and H. J. Bakker, "Influence of pump wavelength and crystal length on the phase matching of optical rectification," J. Opt. Soc. Am. B **22**(8), 1714–1718 (2005).
15. Y. R. Shen, "Principles of Nonlinear Optics," John Wiley & Sons, 1984.
16. D. T. F. Marple, "Refractive index of ZnSe, ZnTe, and CdTe," J. Appl. Phys. **35**(3), 539–542 (1964).
17. Y. Horikoshi, A. Ebina, and T. Takahashi, "Optical Absorption Due to Acceptor Levels in Undoped ZnTe," Jpn. J. Appl. Phys. **11**(7), 992–1001 (1972).
18. G. Gallot, J. Zhang, R. W. McGowan, T.-I. Jeon, and D. Grischkowsky, "Measurements of the THz absorption and dispersion of ZnTe and their relevance to the electro-optic detection of THz radiation," Appl. Phys. Lett. **74**(23), 3450–3452 (1999).
19. M. Schall and P. Uhd Jepsen, "Above-band gap two-photon absorption and its influence on ultrafast carrier dynamics inZnTe and CdTe," Appl. Phys. Lett. **80**(25), 4771–4773 (2002).
20. S. Krishnamurthy, Z. G. Yu, L. P. Gonzalez, and S. Guha, "Temperature- and wavelength-dependent two-photon and free-carrier absorption in GaAs, InP, GaInAs, and InAsP," J. Appl. Phys. **109**(3), 033102 (2011).
21. P. L. Kelley, "Nonlinear effects in solids," J. Phys. Chem. Solids **24**(5), 607–616 (1963).
22. P. L. Kelley, "Second harmonic generation in solids," J. Phys. Chem. Solids **24**(9), 1113–1119 (1963).
23. M. I. Bell, "Frequency dependence of Miller's Rule for nonlinear susceptibilities," Phys. Rev. B **6**(2), 516–521 (1972).
24. D. Bethune, A. J. Schmidt, and Y. R. Shen, "Dispersion of nonlinear optical susceptibilities of InAs, InSb, and GaAs in the visible region," Phys. Rev. B **11**(10), 3867–3875 (1975).
25. J. L. P. Hughes and J. E. Sipe, "Calculation of second-order optical response in semiconductors," Phys. Rev. B **53**(16), 10751–10763 (1996).
26. R. K. Chang, J. Ducuing, and N. Bloembergen, "Dispersion of the Optical Nonlinearity in Semiconductors," Phys. Rev. Lett. **15**(9), 415–418 (1965).
27. F. G. Parsons and R. K. Chang, "Measurement of the nonlinear susceptibility dispersion by dye lasers," Opt. Commun. **3**(3), 173–176 (1971).
28. K. Sato and S. Adachi, "Optical properties of ZnTe," J. Appl. Phys. **73**(2), 926–931 (1993).